arXiv:1007.1827v1 [astro-ph.CO] 12 Jul 2010

Effect of Foregrounds on the CMBR Multipole Alignment

Pavan K. Aluri[1], Pramoda K. Samal[2],
Pankaj Jain[1] and John. P. Ralston[3]

[1]Department of Physics, Indian Institute of Technology, Kanpur 208016, India
[2]Department of Physics, Utkal University, Bhubaneswar, 751004, India
[3] Department of Physics & Astronomy, University of Kansas, Lawrence, KS - 66045, USA

Abstract

We analyze the effect of foregrounds on the observed alignment of CMBR quadrupole and octopole. The alignment between these multipoles is studied by using a symmetry based approach which assigns a principal eigenvector (PEV) or an axis with each multipole. We determine the significance of alignment between these multipoles by using the Internal Linear Combination (ILC) 5 and 7 year maps and also the maps obtained by using the Internal Power Spectrum Estimation (IPSE) procedure. The effect of foreground cleaning is studied in detail within the framework of the IPSE method both analytically and numerically. By using simulated CMBR data, we study how the PEVs of the pure simulated CMB map differ from those of the final cleaned map. We find that, in general, the shift in the PEVs is relatively small and in random directions. Due to the random nature of the shift we conclude that it can only lead to misalignment rather than alignment of multipoles. We also directly estimate the significance of alignment by using simulated cleaned maps. We find that the results in this case are identical to those obtained by simple analytic estimate or by using simulated pure CMB maps.

Keywords: cosmic microwave background, methods: data analysis, methods: statistical

1 Introduction

The standard cosmological model rests on the *Cosmological Principle* which states that the universe is homogeneous and isotropic. However, there are many indications from diverse data sets that this principle may not be applicable. In particular, polarizations of radio waves coming from distant radio galaxies (Birch 1982; Jain and Ralston 1999), the optical polarizations from quasars (Hutsemékers 1998; Hutsemékers and Lamy 2001, Jain et al. 2004) and the multipoles $l = 1, 2, 3$ of Cosmic Microwave Background Radiation (CMBR) all indicate a universal axis pointing in the direction of the Virgo cluster (de Oliveira-Costa et al. 2004; Ralston and Jain 2004; Schwarz et al 2004). This phenomenon has been called the *Virgo Alignment* (Ralston and Jain 2004). There have also been other claims of large scale anisotropy in the CMBR data. These include the dipole power modulation (Eriksen et al. 2004; Eriksen et al. 2007; Hoftuft et al. 2009), as well as, the detection of an anomalously cold spot (Cruz et al. 2005). These anomalies have been studied in great detail (Bielewicz et al. 2004; Hansen et al. 2004; Katz and Weeks 2004; Bielewicz et al. 2005; Prunet et al 2005; Bernui et al. 2006; Copi et al. 2006; Copi et al. 2007; de Oliveira-Costa and Tegmark 2006; Wiaux et al. 2006; Freeman et al. 2006; Helling et al. 2006; Bernui et al. 2007; Land and Magueijo 2007; Magueijo and Sorkin 2007). Meanwhile some studies do not find any violation of statistical isotropy in CMB (Hajian et al. 2005; Hajian and Souradeep 2006). Furthermore, the cluster peculiar velocities (Kashlinsky et al. 2008, 2009), as well as the large scale galaxy distribution (Itoh et al. 2009), also indicate deviations from isotropy. The preferred axis for the cluster peculiar velocities with a high redshift cut is again found to be close to the direction of Virgo cluster. In the galaxy distribution surveys, the preferred axis appears to depend strongly on the cut made on the data.

There have been a variety of proposals in the literature explaining the possible origin of this *alignment anomaly*, such as, anisotropic space-times (Berera et al. 2004; Kahniashvili et al. 2008), foreground contaminations (Slosar and Seljak 2004; Abramo et al. 2006; Rakic et al. 2006), noise bias or systematics (Naselsky et al. 2008), vector like dark energy (Armendariz-Picon 2004), spontaneous breaking of isotropy (Gordon et al. 2005; Land and Magueijo 2006, Erickcek et al. 2009), inhomogeneous universe (Moffat 2005; Land and Magueijo 2006), inhomogeneous inflation (Carroll et al. 2010), violation of rotational invariance during inflation (Ackerman et al. 2009), anisotropic perturbations due to dark energy (Battye and Moss 2006), anisotropic inflation (Buniy et al. 2006), local voids (Inoue and Silk 2006) and anisotropic dark energy (Koivisto and Mota 2008; Rodrigues 2008).

Another interesting effect associated with quadrupole is its low power in

comparison to the best fit LCDM model (Bennett et al. 2003). One may speculate that the observed quadrupole-octopole alignment is related to the observed low quadrupole power. It has been shown that in random realizations of pure CMB maps there is no correlation between the low quadrupole power and quadrupole-octopole alignment (Rakić and Schwarz 2007; Sarkar et al. 2010).

In the present paper, we analyze the alignment of CMBR quadrupole ($l = 2$) and octopole ($l = 3$) moments more closely. In (Slosar and Seljak 2004), it has been suggested that this alignment may be caused by the galactic foregrounds. These authors argue that most of the power of quadrupole and octopole lies in the most contaminated region of the sky. Hence, it is entirely possible that these multipoles may be significantly contaminated and the alignment may be caused due to poor cleaning.

In the Internal Power Spectrum Estimation (IPSE) procedure (Saha et al. 2006, 2008; Samal et al. 2010) the cleaning is performed by a totally blind procedure without making any explicit model for foregrounds. The foregrounds are removed by adding maps, in harmonic space, at different frequencies with suitable weights, chosen so as to minimize the foreground power. The Internal Linear Combination (ILC) map provided by the WMAP team (Bennett et al. 2003) also uses a similar cleaning procedure. Here the weighted maps are added directly in pixel space. Both of these procedures are highly effective in removing foregrounds. However some residual foregrounds may still contaminate the data. Besides this, (Saha et al. 2008; Samal et al. 2010) pointed out the existence of bias in the low l multipoles extracted from foreground cleaned maps. This bias leads to a significant reduction of extracted power in these multipoles. In fact, the bias completely explains the observed low power at $l = 2$, in comparison to the best fit theoretical LCDM model. It is clearly important to determine what the low l bias might imply for the alignment of these multipoles. It is possible that the power gets eliminated in just the precise manner in order to cause alignment. Here we study whether any of these residual effects, present in the foreground cleaned data, may cause the observed quadrupole-octopole alignment.

It is important to note that the observed alignment is only getting better with more data. A larger data sample implies smaller uncertainties due to detector noise. Hence the signal becomes more prominent as the fluctuations due to detector noise get suppressed.

The problem of testing violation of isotropy in the CMBR signal has been addressed by many authors. The CMBR anisotropy spectrum is generally assumed to be isotropic in a statistical sense. The assumption of statistical isotropy of the CMBR signal means that the spectral coefficients, a_{lm}, are

uncorrelated for different m and l, i.e. the ensemble average,

$$< a^*_{lm} a_{l'm'} >= \delta_{ll'}\delta_{mm'} C_l \,, \tag{1}$$

where C_l is the standard power. A multitude of statistics have been proposed in order to test for deviation from statistical isotropy in the CMBR data (Hajian et al. 2005; Hajian and Souradeep 2006; Copi et al. 2006, 2007). Here we shall use the method introduced in (Ralston and Jain 2004) and further developed in (Samal et al. 2008, 2009). In this procedure, one assigns three orthogonal unit vectors for each multipole. The orientation of these vectors as well as the power associated with each vector contains information about possible violation of statistical isotropy. This information is encoded in two entropy measures, the power entropy and alignment entropy, defined in (Samal et al. 2008). Using this method one can test for violation of isotropy for each individual multipoles or collectively over a range of multipoles. We present an outline of our analysis procedure in the next section followed by results from cosmological data and simulations and conclusions in the end.

2 Analysis Methodology

The primary objective of the present paper is to determine whether the alignment of quadrupole and octopole can be caused by foreground contamination. The alignment of different multipoles can be quantified by associating a frame with each multipole (Ralston and Jain 2004; Samal et al. 2008). In order to analyse the effect of foreground contamination we first perform an analytic calculation of the power tensor, introduced in (Ralston and Jain 2004; Samal et al. 2008), within the framework of IPSE technique (Saha et al. 2006, 2008; Samal et al. 2010). Here we confine ourselves to the simple case of one foreground component following rigid frequency scaling and two frequency bands. This computation is useful to determine if the low l bias also leads to violation of statistical isotropy. We then numerically determine the effect of this bias and residual foregrounds on the alignment of quadrupole and octopole. We generate many random realizations of the CMBR maps including foregrounds and detector noise. We use the Planck Sky Model (PSM)[3] for foregrounds and use all the five WMAP frequency bands. These simulated raw maps are cleaned using the IPSE technique. We study the difference in the extracted principal eigenvectors of cleaned maps and simulated pure CMB maps. This allows us to determine if the residual foregrounds lead to any preferential alignment of these extracted vectors.

[3]http://www.planck.fr/heading79.html

In the next subsections, we briefly review the extraction of frames and the IPSE technique.

2.1 Covariant frames

The present study utilizes a symmetry based statistic (Samal et al. 2008) to test for statistical isotropy in the CMBR data. The method associates a wave function ψ^k_m, defined as,

$$\psi^k_m(l) = \frac{1}{\sqrt{l(l+1)}}\langle l, m|J^k|a(l)\rangle \tag{2}$$

with every multipole l. Here $|a(l)\rangle$ contains information about the spectral moments, such that,

$$a_{lm} = \langle l, m|a(l)\rangle \tag{3}$$

where $|lm\rangle$ are the eigenstates of the angular momentum operators $\vec{J}^2$, J_z in the spin-l representation. The wave function ψ^k_m is useful since it assigns a frame, i.e. three orthonormal vectors, at each l. The frame may be extracted by making a singular value decomposition of the wave function.

It is also convenient to define the power tensor,

$$\begin{aligned} A_{ij}(l) &= \sum_m \psi^i_m {\psi^j_m}^* \\ &= \frac{1}{l(l+1)} \sum_{m,m'} a^*_{lm}(J_iJ_j)_{mm'}a_{lm'}\,. \end{aligned} \tag{4}$$

The three eigenvectors, e^α_i, $\alpha = 1, 2, 3$, of this matrix define the frame associated with each multipole. The index, $i = 1, 2, 3$, labels the three components of each eigenvector. The corresponding eigenvalues, $(\Lambda^\alpha)^2$, contain information about the power associated with each eigenvector. The sum of the three eigenvalues equals the total power, C_l. A large dispersion in the eigenvalues indicates violation of statistical isotropy for a particular mode.

We define the principal pigenvector (PEV), $\hat{n}_l$, as the eigenvector corresponding to the maximum eigenvalue. Here we note that the extracted PEVs are headless, meaning, these vectors specify only an axis and not a direction. The P-value or the significance of alignment of the quadrupole and octopole PEV may be estimated analytically by the formula $P = 1-\hat{n}_2\cdot\hat{n}_3 = 1 - \cos(\delta\Theta)$. Here $\delta\Theta$ is the angle between the PEVs $\hat{n}_2$ and $\hat{n}_3$, which correspond to $l = 2$ and $l = 3$ respectively. Alternatively, one can estimate the significance directly by numerical simulations, as described below.

2.2 IPSE method

The IPSE procedure removes the foreground contamination by linearly combining maps at different frequencies with suitable weights in harmonic space. The cleaning is accomplished independently for each l. Let $\hat{w}_l^a$ denote the weights for the map at frequency channel a corresponding to the multipole l. In case we have several maps at a particular frequency, we simply take their average. The spherical harmonic components of the cleaned map are given by,

$$a_{lm}^{\rm Clean} = \sum_{a=1}^{n_c} \hat{w}_l^a \frac{a_{lm}^a}{B_l^a} \,. \tag{5}$$

Here n_c is the total number of frequency channels used for cleaning. The factor B_l^a is the circularized beam transform function at frequency band a (Hill et al. 2008). The a_{lm}^a represent the harmonic coefficients of the observed map. It can be expressed as

$$a_{lm}^a = (a_{lm}^s + a_{lm}^{(f)a}) B_l^a + a_{lm}^{(N)a} \tag{6}$$

where a_{lm}^s, $a_{lm}^{(f)a}$ and $a_{lm}^{(N)a}$ represent the contributions from CMB, foregrounds and detector noise respectively at frequency channel a.

The weights $\hat{w}_l^a$ are obtained by minimizing the total power subject to the constraint

$$\hat{\mathbf{W}}_l \mathbf{e}_0 = \mathbf{e}_0^T \hat{\mathbf{W}}_l^T = 1 \,, \tag{7}$$

where $\mathbf{e}_0$ is a column vector with unit elements

$$\mathbf{e}_0 = \begin{pmatrix} 1 \\ .. \\ .. \\ 1 \end{pmatrix} \,, \tag{8}$$

and $\hat{\mathbf{W}}_l$ is the row vector $(\hat{w}_l^1, \hat{w}_l^2, .., \hat{w}_l^{n_c})$. This gives

$$\hat{\mathbf{W}}_l = \frac{\mathbf{e}_0^T \hat{\mathbf{C}}_l^{-1}}{\mathbf{e}_0^T \hat{\mathbf{C}}_l^{-1} \mathbf{e}_0} \,, \tag{9}$$

where $\hat{\mathbf{C}}_l$ is the empirical covariance matrix (Tegmark and Efstathiou 1996; Tegmark et al. 2003; Saha et al. 2006; Delabrouille and Cardoso 2009). Its ab matrix element may be expressed as, $\hat{C}_l^{ab}/(B_l^a B_l^b)$, where $\hat{C}_l^{ab}$ is the cross power spectrum between the a^{th} and b^{th} channel,

$$\hat{C}_l^{ab} = \sum_{m=-l}^{m=l} \frac{a_{lm}^a a_{lm}^{b*}}{2l+1} \,. \tag{10}$$

The final cleaned map may be used to extract the power spectrum as well as the PEVs needed for the present study. The power spectrum is given by,

$$\hat{C}_l^{Clean} = \frac{1}{\mathbf{e}_0^T \hat{\mathbf{C}}_l^{-1} \mathbf{e}_0} \,. \tag{11}$$

This would be reliable at low l, where the detector noise is negligible. For our present purpose, this is sufficient. However at high $l > 200$, where the detector noise is not negligible, a more elaborate procedure is necessary, as discussed in (Saha et al. 2008).

The procedure contains some bias which can be estimated from simulations. An important bias arises due to inefficient cleaning in the galactic plane. A similar bias is also present in the procedure used by WMAP science team in generating the ILC map. As a final step in generating this map, a 'bias' correction based on Monte Carlo simulations is applied by the WMAP science team (Hinshaw et al. 2007). We employ a similar procedure to correct for any residual foreground bias by subtracting a 'bias map' generated from the simulated maps, in pixel space.

Another interesting bias arises due to the cross correlation term between the foregrounds and the CMB signal in the calculation of CMB power. This bias is negative and affects dominantly the very low multipoles. This can also be estimated by simulations, but may also be represented analytically by using some simplifying assumptions (Saha et al. 2008).

2.3 Simulations

In order to study the effect of foregrounds on the detected anisotropy in CMBR, we generate an ensemble of 500 CMB maps as random realizations of the best fit theoretical power spectrum, available at the NASA's WMAP public domain website[1]. These simulated "pure" CMB maps are generated using the publicly available HEALPix software[2]. Eventually, these pure CMB maps are contaminated with galactic foregrounds and gaussian random noise with appropriate dispersion per pixel. The foregrounds are generated using the PSM, which contains only thermal dust, synchrotron and free-free emission. These are the dominant foregrounds, as characterised by WMAP science team also, in all its data releases so far (Gold et al. 2010). The effective number of observations needed to generate the noise maps are taken from temperature maps of WMAP 5 year and 7 year data releases, available in FITS format at NASA's LAMBDA website[1]. These simulated CMB maps

[1]http://lambda.gsfc.nasa.gov/
[2]http://healpix.jpl.nasa.gov/

are then passed through a cleaning pipeline using the IPSE procedure. This produces a full sky cleaned map corresponding to each random realization which can be used to study the alignment between quadrupole and octopole. By comparing observations with the random samples, we can easily estimate the significance level of the observed alignment. Furthermore, we can study how the PEVs in the extracted clean CMB maps differ from those of pure CMB maps. This can reveal any systematic bias which may be present in the PEVs of cleaned maps. Due to the presence of residual foregrounds and negative bias at low l, we expect that the corresponding eigenvectors may also be biased. Here we shall study this bias and its effect on alignment of quadrupole and octopole.

3 Effect of low-l bias

In this section we evaluate analytically how the low-l negative bias affects the power tensor. For simplicity we assume that there is only one significant foreground component, which follows rigid frequency scaling. Furthermore we assume only two frequency bands in the CMB data analysis. The detector noise is assumed to be negligible, which is a reasonable assumption at low-l. For simplicity we also set the beam transform function to unity. We compute the ensemble average of the power tensor within the framework of the IPSE method using these simplifying assumptions.

The wave function $\psi^i_m(l)$ associated with each multipole, Eq. 2, may be expressed as,

$$\psi^i_m(l) \;=\; \frac{1}{\sqrt{l(l+1)}}\sum_{m'}\langle lm|J_i|lm'\rangle a_{lm'}\ . \tag{12}$$

The corresponding power tensor may be written as,

$$A_{ij}(l) \;=\; \frac{1}{l(l+1)}\sum_{m,m',m''}\langle lm|J_i|lm'\rangle\langle lm''|J_j|lm\rangle a_{lm'}a^*_{lm''}\,. \tag{13}$$

To calculate the bias in the power tensor we take its ensemble average, to get,

$$\langle A_{ij}(l)\rangle_{ens.avg.} = \frac{1}{l(l+1)}\sum_{m,m',m''}\langle lm|J_i|lm'\rangle\langle lm''|J_j|lm\rangle\langle a_{lm'}a^*_{lm''}\rangle_{ens.avg.}\,, \tag{14}$$

where the symbol $<>_{ens.avg.}$ denotes ensemble average. It follows from the *Cosmological principle* that the fluctuations in CMBR are statistically isotropic.

Hence we expect for a pure CMB map,

$$\langle A_{ij}(l)\rangle_{ens.avg.} = \frac{C_l}{3}\delta_{ij}\,. \tag{15}$$

Here we compute the ensemble average of the power tensor for the cleaned map. This will show us whether the bias generated due to foreground cleaning leads to anisotropy in the power tensor.

The spherical harmonic coefficients of a cleaned map can be written as,

$$a_{lm}^{Clean} = a_{lm}^{(s)} + a_{lm}^{res}\,, \tag{16}$$

where a_{lm}^{res} denotes any residual foreground contamination in the cleaned map,

$$a_{lm}^{res} = \sum_{b=1}^{n_c} \hat{w}_l^b a_{lm}^{(f)b}\,. \tag{17}$$

In order to estimate the bias in power tensor, we need to calculate,

$$\begin{aligned}
\langle a_{lm'}^{Clean} a_{lm''}^{Clean*}\rangle_{ens.avg.} &= \left\langle \left(a_{lm'}^{(s)} + \sum_{b=1}^{n_c} \hat{w}_l^b a_{lm'}^{(f)b}\right)\left(a_{lm''}^{(s)} + \sum_{b'=1}^{n_c} \hat{w}_l^{b'} a_{lm''}^{(f)b'}\right)^*\right\rangle \\
&= C_l^{(s)}\delta_{m'm''} + \langle a_{lm'}^{(s)}\hat{w}_l^{b'} a_{lm''}^{(f)b'*}\rangle + \langle a_{lm''}^{(s)\,*}\hat{w}_l^b a_{lm'}^{(f)b}\rangle + \\
&\quad + \langle \hat{w}_l^b a_{lm'}^{(f)b} a_{lm''}^{(f)b'*}\hat{w}_l^{b'}\rangle\,.
\end{aligned} \tag{18}$$

The first term follows from the assumption that CMB signal is statistically isotropic. The frequency band indices b and b' in the second, third and fourth terms after second equality are summed over as in Einstein's convention.

The elements of the empirical covariance matrix are given by,

$$\begin{aligned}
\hat{C}_l^{ab} &= \frac{1}{2l+1}\sum_{m=-l}^{+l} a_{lm}^a a_{lm}^{b*} \\
&= \frac{1}{2l+1}\sum_{m=-l}^{+l}\left(a_{lm}^{(s)} + a_{lm}^{(f)a}\right)\left(a_{lm}^{(s)} + a_{lm}^{(f)b}\right)^* \\
&= \hat{C}_l^{(s)} + \hat{C}_l^{(s)(f)a} + \hat{C}_l^{(s)(f)b} + C_l^{(f)a(f)b}\,.
\end{aligned} \tag{19}$$

We get the last line after carrying out the multiplications in the second line and $\hat{C}_l^{(s)(f)a}$ and $\hat{C}_l^{(s)(f)b}$ denote cross correlations between the CMB and foregrounds at frequency bands a and b, respectively. Note that, these quantities vanish on an ensemble average, as CMB and foregrounds are uncorrelated with one another i.e., $\langle C_l^{(s)(f)a}\rangle = 0 = \langle C_l^{(s)(f)b}\rangle$. However, for a particular realization these quantities need not vanish.

As mentioned above we make the estimate of bias in power tensor assuming a single foreground component and 2 frequency channels. Thus, the empirical covariance matrix reads as,

$$\hat{\mathbf{C}}_l = \begin{pmatrix} \hat{C}_l^{(s)} + 2\hat{C}_l^{(s)(f)1} + C_l^{(f)1} & \hat{C}_l^{(s)} + \hat{C}_l^{(s)(f)1} + \hat{C}_l^{(s)(f)2} + C_l^{(f)1(f)2} \\ \hat{C}_l^{(s)} + \hat{C}_l^{(s)(f)1} + \hat{C}_l^{(s)(f)2} + C_l^{(f)1(f)2} & \hat{C}_l^{(s)} + 2\hat{C}_l^{(s)(f)2} + C_l^{(f)2} \end{pmatrix} . \quad (20)$$

Hence,

$$\hat{\mathbf{C}}_l^{-1} = \frac{1}{\hat{\Delta}} \begin{pmatrix} \hat{C}_l^{(s)} + 2\hat{C}_l^{(s)(f)2} + C_l^{(f)2} & -\left(\hat{C}_l^{(s)} + \hat{C}_l^{(s)(f)1} + \hat{C}_l^{(s)(f)2} + C_l^{(f)1(f)2}\right) \\ -\left(\hat{C}_l^{(s)} + \hat{C}_l^{(s)(f)1} + \hat{C}_l^{(s)(f)2} + C_l^{(f)1(f)2}\right) & \hat{C}_l^{(s)} + 2\hat{C}_l^{(s)(f)1} + C_l^{(f)1} \end{pmatrix} , \quad (21)$$

where $\hat{\Delta}$ denotes the determinant of $\hat{\mathbf{C}}_l$. Using the above result we compute $\mathbf{e}_0^T \hat{\mathbf{C}}_l^{-1} \mathbf{e}_0$ to get the cleaned map power spectrum as

$$\begin{aligned} \hat{C}_l^{Clean} &= \frac{\hat{\Delta}}{C_l^{(f)1} + C_l^{(f)2} - 2C_l^{(f)1(f)2}} \\ &= \hat{C}_l^{(s)} + \frac{1}{\delta}\Big[2\hat{C}_l^{(s)(f)1} C_l^{(f)2} + 2C_l^{(s)(f)2}\hat{C}_l^{(f)1} + C_l^{(f)1} C_l^{(f)2} - \\ &\quad - (C_l^{(f)1(f)2})^2 - 2C_l^{(f)1(f)2}\left(\hat{C}_l^{(s)(f)1} + \hat{C}_l^{(s)(f)2}\right) \\ &\quad - (\hat{C}_l^{(s)(f)1})^2 - (\hat{C}_l^{(s)(f)2})^2 + 2\hat{C}_l^{(s)(f)1}\hat{C}_l^{(s)(f)2}\Big] \end{aligned} \quad (22)$$

and the corresponding weights,

$$\begin{aligned} \hat{\mathbf{W}}_l &= \frac{\mathbf{e}_0^T \hat{\mathbf{C}}_l^{-1}}{\mathbf{e}_0^T \hat{\mathbf{C}}_l^{-1} \mathbf{e}_0} \\ &= \frac{1}{\delta}\begin{bmatrix} -\hat{C}_l^{(s)(f)1} + \hat{C}_l^{(s)(f)2} - C_l^{(f)1(f)2} + C_l^{(f)2} \\ \hat{C}_l^{(s)(f)1} - \hat{C}_l^{(s)(f)2} - C_l^{(f)1(f)2} + C_l^{(f)1} \end{bmatrix} . \end{aligned} \quad (23)$$

The term δ in the denominator of Eq. 22 and Eq. 23 is $\delta = C_l^{(f)1} + C_l^{(f)2} - 2C_l^{(f)1(f)2}$. We next calculate all the terms in Eq. 18 one by one. First, consider the second term in second line of Eq. 18:

$$a_{lm'}^{(s)} \hat{w}_l^{b'} a_{lm''}^{(f)b'*} = a_{lm'}^{(s)} \hat{w}_l^1 a_{lm''}^{(f)1*} + a_{lm'}^{(s)} \hat{w}_l^2 a_{lm''}^{(f)2*} \quad (24)$$

Using Eq. 23 in Eq. 24 and then taking an ensemble average, we get,

$$\begin{aligned} \langle a_{lm'}^{(s)} \hat{w}_l^{b'} a_{lm''}^{(f)b'*} \rangle &= \frac{C_l^{(s)}}{(2l+1)\delta}\Big[-a_{lm'}^{(f)1} a_{lm''}^{(f)1*} + a_{lm'}^{(f)1} a_{lm''}^{(f)2*} \\ &\quad + a_{lm'}^{(f)2} a_{lm''}^{(f)1*} - a_{lm'}^{(f)2} a_{lm''}^{(f)2*}\Big] . \end{aligned} \quad (25)$$

To proceed further we assume that the foreground component follows rigid frequency scaling. In astrophysical applications, the map of any foreground component at a frequency ν is generally modelled as,

$$F(\hat{n}) = A_{\nu_0}(\hat{n}) \left(\frac{\nu}{\nu_0}\right)^{-\beta(\hat{n})} , \tag{26}$$

where A_{ν_0} is the observed foreground template at certain reference frequency ν_0 and $\beta(\hat{n})$ denotes spectral index of the foreground component. A foreground for which the approximation of a constant value of β over the entire sky holds is said to follow rigid frequency scaling, though, in a most general case β is a function of position of the sky, $\hat{n}$. If for a foreground, the assumption of constant β is not reasonable, one can model the variation in terms of two components each of which follows rigid scaling (Bouchet and Gispert 1999). So, in that case,

$$F(\hat{n}) = A_{\nu_0} \left(\frac{\nu}{\nu_0}\right)^{-\overline{\beta}} + B_{\nu_0}(\hat{n}) \left(\frac{\nu}{\nu_0}\right)^{-\overline{\beta}} \ln(\nu/\nu_0) , \tag{27}$$

where $\overline{\beta}$ denotes average spectral index of the foreground, $F(\hat{n})$, over the entire sky and A, B are two templates of the foreground. A very strong variation may require more than two templates for modelling.

Here, assuming a rigid scaling behaviour for the foreground component, we model the spectral coefficients of the foreground in a frequency band b as,

$$a_{lm}^{(f)b} = A_{lm} \left(\frac{1}{f_b}\right)^{\alpha} . \tag{28}$$

Now, Eq. 25 becomes,

$$\langle a_{lm'}^{(s)} \hat{w}_l^{b'} a_{lm''}^{(f)b'*} \rangle = -A_{lm'} A_{lm''}^{*} \frac{C_l^{(s)}}{(2l+1)\delta} \left(\frac{1}{f_1^{\alpha}} - \frac{1}{f_2^{\alpha}}\right)^2 . \tag{29}$$

The third term after second equality in Eq. 18 is same as the second term. The fourth term is,

$$\begin{aligned} \langle \hat{w}_l^b a_{lm'}^{(f)b} a_{lm''}^{(f)b'*} \hat{w}_l^{b'} \rangle &= \left\langle \left(\hat{w}_l^1 a_{lm'}^{(f)1} + \hat{w}_l^2 a_{lm'}^{(f)2}\right) \left(\hat{w}_l^1 a_{lm''}^{(f)1} + \hat{w}_l^2 a_{lm''}^{(f)2}\right)^* \right\rangle \\ &= \langle (\hat{w}_l^1)^2 \rangle a_{lm'}^{(f)1} a_{lm''}^{(f)1*} + 2\langle \hat{w}_l^1 \hat{w}_l^2 \rangle a_{lm'}^{(f)1} a_{lm''}^{(f)2*} \\ &\quad + \langle (\hat{w}_l^1)^2 \rangle a_{lm'}^{(f)2} a_{lm''}^{(f)2*} . \end{aligned} \tag{30}$$

With rigid scaling approximation for the foreground and after a lengthy algebra, we finally get,

$$\langle \hat{w}_l^b a_{lm'}^{(f)b} a_{lm''}^{(f)b'*} \hat{w}_l^{b'} \rangle = A_{lm'} A_{lm''}^{*} \frac{C_l^{(s)}}{(2l+1)\delta} \left(\frac{1}{f_1^{\alpha}} - \frac{1}{f_2^{\alpha}}\right)^2 . \tag{31}$$

Here we have used,

$$\delta = C_l^{(f)1} + C_l^{(f)2} - 2C_l^{(f)1(f)2} = \frac{1}{2l+1}\sum_{m=-l}^{m=+l} |A_{lm}|^2 \left(\frac{1}{f_1^\alpha} - \frac{1}{f_2^\alpha}\right)^2 .$$

Finally we get from Eq. 18,

$$\langle a_{lm'}^{Clean} a_{lm''}^{Clean*} \rangle = C_l^{(s)} \delta_{m'm''} - C_l^{(s)} A_{lm'} A_{lm''}^* \left(\sum_{m=-l}^{m=+l} |A_{lm}|^2\right)^{-1} . \qquad (32)$$

Hence we find that the low-l negative bias term leads to an anisotropic power tensor. As discussed in (Saha et al. 2008; Samal et al. 2010) this bias arises even in the case of perfect cleaning, where we have enough frequency channels to remove all the foregrounds. Besides this term we also expect a positive contribution due to residual foreground contamination. This arises due to foregrounds which may not be eliminated by our cleaning procedure. By explicit numerical computation we find that the PEV of the power tensor corresponding to Eq. 32 is well aligned with the galactic poles. The two orthogonal vectors of the power tensor lie in the galactic plane. This is of course expected since the eigenvectors are determined entirely by the galactic foregrounds, which are present predominantly along the galactic plane.

The main result of this section is that power tensor corresponding to the cleaned map acquires an anisotropic contribution due to low-l negative bias. This contribution arises even in the case of perfect cleaning when we have sufficient frequency channels to remove all the foregrounds present in the data. Although we have made several simplifying assumptions, this basic result is expected to hold in general. Our analytic results in this section, however, do not provide any guidance on how the PEV is affected due to foreground cleaning. In the next section we estimate the total bias in the PEV by direct simulations.

4 Results

4.1 Observational data

We, first, present the results from actual cosmological data and then discuss the simulation results. The PEVs, $\hat{n}_2$ and $\hat{n}_3$, for the quadrupole and octopole, respectively, from different clean maps extracted from the WMAP data are given in Table [1]. The results presented here are for the WMAP ILC maps and the IPSE cleaned maps, with and without bias correction,

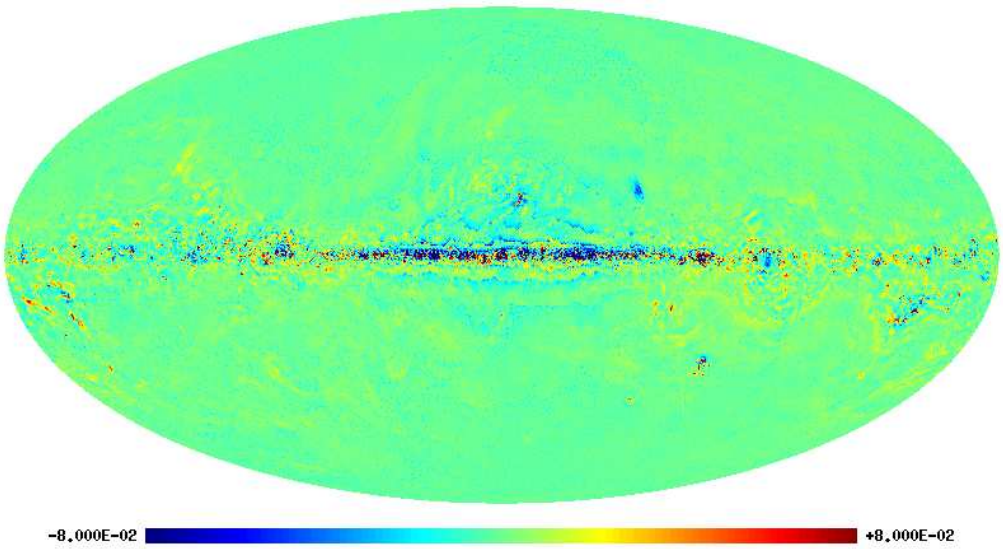

Figure 1: The bias map for seven year data generated using the IPSE procedure.

for both five and seven year data sets. The bias map, generated from Monte Carlo simulations of 500 random realizations, is shown in Fig. [1]. The power spectrum corresponding to this bias map is shown in Fig. [2]. As expected, we see that the bias correction is present, predominantly, in the galactic plane and is almost zero away from it. We point out that this bias is completely different from the negative bias discussed in the previous section.

The ILC map is obtained by linearly combining the temperature maps, observed in different frequency bands, in real space, with appropriate weights to remove the foregrounds. In contrast, the IPSE map is obtained by making linear combinations in harmonic space. We point out that, the bias removal leads to a significantly improved cleaning in the galactic plane and has already been applied in the publicly available ILC map. The angle, $\delta\Theta$, between the two axes, $\hat{n}_2$ and $\hat{n}_3$, for different foreground cleaned maps, is listed in Table 2. Here, we also list the analytic estimate of probability for the alignment found in WMAP CMBR data to be a random occurrence.

We find that, the alignment between quadrupole and octopole is striking in both the ILC five and seven year maps. We also note that, in WMAP 3 year ILC map, the alignment of quadrupole and octopole is found to be 5.51^o, which has a random occurrence probability of 0.0051. So, with more data release, the alignment appears to be getting better. The significance for the observed alignment in seven year data is better than 4σ. The IPSE cleaned, bias corrected 7 year map gives significance close to 3σ. In comparison,

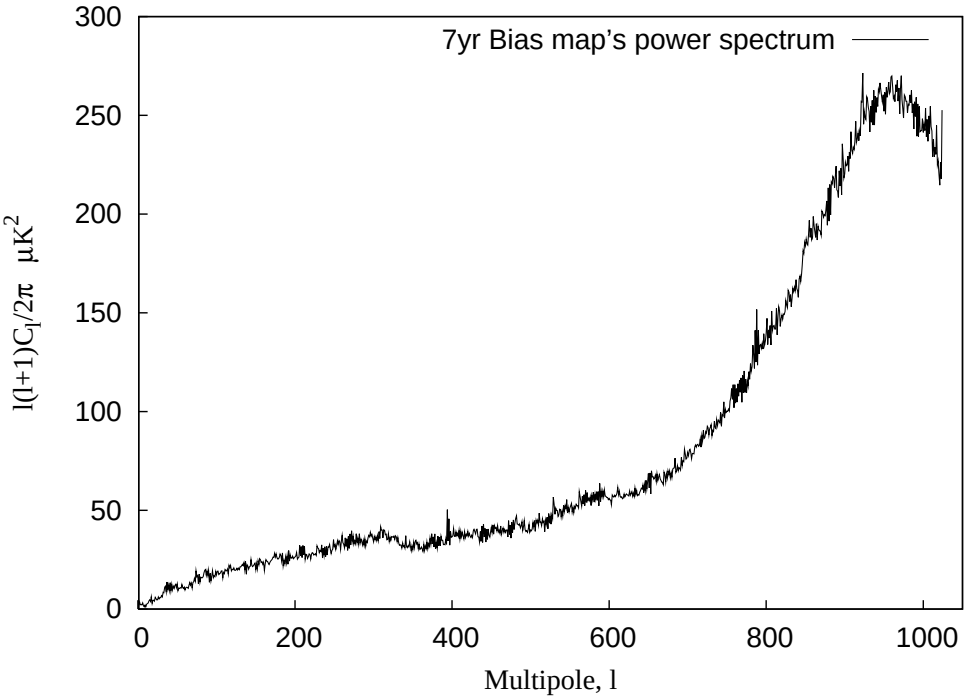

Figure 2: The power spectrum of the bias map shown in Fig. [1].

the IPSE map without bias correction gives a much poorer alignment with $\delta\Theta = 11.28^o$(a 98.1% CL). The main difference between these two maps is that a significant foreground contamination in the galactic plane has been removed during the process of bias removal. This suggests that the effect of foregrounds is to distort the signal of alignment rather than to cause alignment.

We also notice from Table[1] that, as we remove the bias in the IPSE map, the octopole PEV changes only by a negligible amount, whereas the quadrupole undergoes a significantly large change. Indeed, after bias removal, the quadrupole PEV is relatively close to that corresponding to the ILC map. The IPSE octopole PEV agrees well with that obtained from ILC map, irrespective of whether the bias is removed or not. So, it seems that quadrupole is more susceptible to distortion due to the presence of residual foregrounds.

4.2 Simulation Results

We next use simulated CMB maps to determine the effect of foreground cleaning on the properties of the extracted CMB signal. The simulated maps

	$\hat{n}_2$	$\hat{n}_3$
WMAP ILC map (5 yr)	$(0.2458, 0.4135, -0.8767)$	$(0.2505, 0.3823, -0.8895)$
WMAP ILC map (7 yr)	$(0.2484, 0.3921, -0.8857)$	$(0.2434, 0.3842, -0.8906)$
IPSE cleaned map (5 yr)	$(0.1481, 0.1923, -0.9701)$	$(0.2040, 0.3863, -0.8996)$
Bias corrected IPSE map (5 yr)	$(0.2936, 0.4091, -0.8640)$	$(0.2086, 0.3855, -0.8988)$
IPSE cleaned map (7yr)	$(0.1355, 0.1957, -0.9713)$	$(0.1782, 0.3773, -0.9088)$
Bias corrected IPSE map (7 yr)	$(0.2301, 0.3240, -0.9176)$	$(0.1773, 0.3754, -0.9097)$

Table 1: The principal eigenvectors (PEVs) $\hat{n}_2$ and $\hat{n}_3$ for quadrupole and octopole, respectively, for different cleaned maps

	$\delta\Theta$	$1 - \cos(\delta\Theta)$
WMAP ILC map (5 yr)	1.95^o	0.00058
WMAP ILC map (7 yr)	0.6^o	5.5×10^{-5}
IPSE cleaned map (5 yr)	12.27^o	0.023
Bias corrected IPSE map (5 yr)	5.44^o	0.0045
IPSE cleaned map (7 yr)	11.28^o	0.019
Bias corrected IPSE map (7 yr)	4.25^o	0.0027

Table 2: Alignment between quadrupole and octopole for different cleaned maps. Also listed are the analytic estimates of the probability for a random occurrence of the observed alignments.

containing CMB, foregrounds and detector noise are cleaned using the IPSE procedure. In each of the simulated maps, the bias due to foreground power in the galactic plane is removed in exactly the same manner as in the real data. Even after removing this bias, we expect that the PEV extracted from the cleaned map may not be exactly the same as that corresponding to the pure CMB map.

Let α be the angle between the pure map PEV ($\hat{n}_p$) and cleaned map PEV ($\hat{n}_c$) for a particular multipole. Here, we are interested only in the quadrupole and the octopole. We call this change in position of pure map PEVs as "rotation" of PEVs in the presence of foregrounds. We want to find out whether there exists any preferred alignment of the pure map PEVs along a particular direction in the presence of foregrounds. In Fig. [3], we show the distribution of "$1 - \cos(\alpha)$", which is a convenient measure of the rotation of the PEVs. One can readily see from the graph that most of the PEVs do not undergo any significant shift. In fact, the number of PEVs which got rotated beyond a cutoff of $1 - \cos(\alpha) = 0.15$ are 52 for l=2, and 30 for l=3, out of the 500 bias corrected clean maps. Hence, the error introduced due to foregrounds on the extraction of the PEVs is generally small.

Fig. [4] shows the plot of "$1-\cos(\alpha)$", for all the 500 simulated maps, as a function of the polar angle, θ, of the pure map PEV, both for $l = 2$ and $l = 3$. Notice the clustering of data points near the zero of y-axis in this plot, which indicates only a very nominal shift in most of the PEVs. It also shows that the PEVs which were lying, initially, in the galactic plane generally undergo larger rotation whereas the effect is small on PEVs at higher latitudes. Note that the galactic foregrounds extend roughly upto 30^o on either side of the galactic equator and are distributed asymmetrically. Next, in Fig. [5] we show the distribution of PEVs in different sky regions for $l = 2$ and $l = 3$. The histograms are shown for both pure and cleaned maps in an interval of 30^o of polar angle across the sky. The distribution of pure map PEVs is relatively flat, as expected. However, the foreground cleaned maps show a dip near the galactic plane. This illustrates that in the cleaned maps the PEVs have a tendency to rotate away from the galactic plane. This effect is seen to be more pronounced in the case of quadrupole in comparison to octopole. The effect is easily understood since the region of the galactic plane is most contaminated by foregrounds. Hence the PEVs in the galactic plane are naturally expected to undergo larger rotation.

Next, we look at the alignment of quadrupole and octople in both pure and cleaned maps. Fig. [6] shows the distribution of "$1 - \cos(\alpha_{23})$", where α_{23} is the angle between the quadrupole and the octopole. The data is binned with a bin size of 0.2. We can easily infer from the figure that these alignments are completely random. Hence, we find no evidence for foregrounds induced

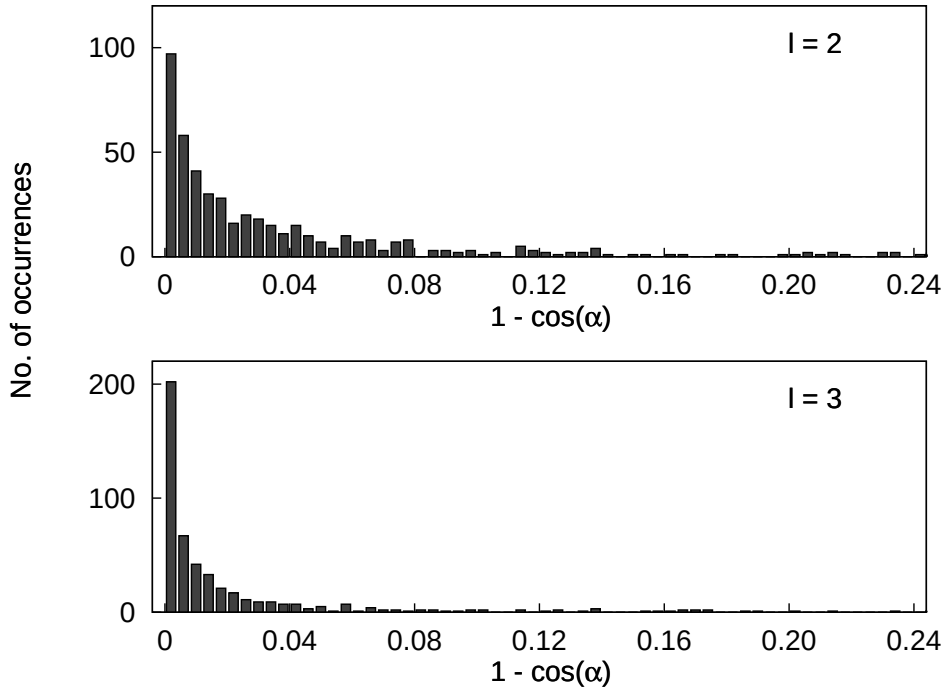

Figure 3: Distribution of $(1 - \cos\alpha)$, where α is the angle between the PEV of simulated pure CMB maps and bias corrected cleaned maps for $l = 2$ and $l = 3$.

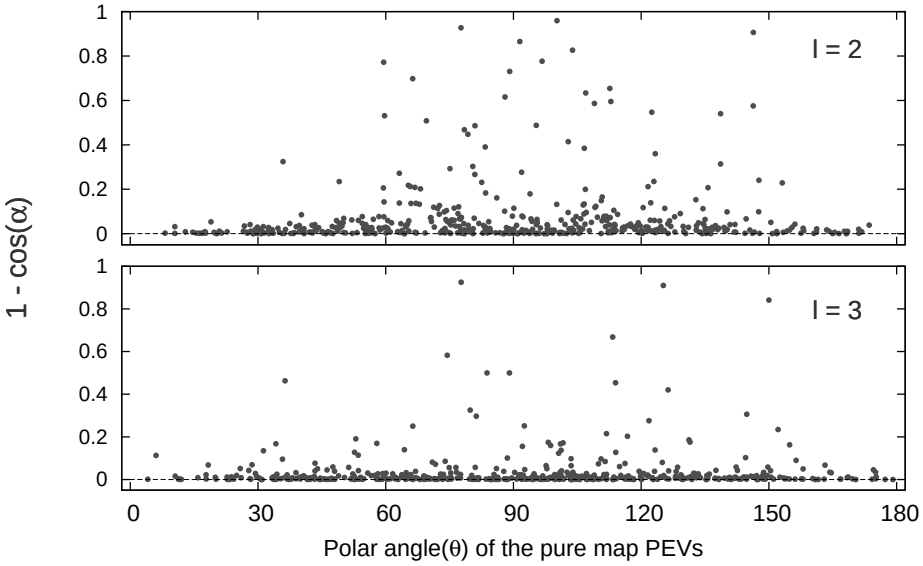

Figure 4: Plot of $(1 - \cos\alpha)$, as a function of polar angle, θ, of pure map PEVs. Here, α is the angle between the PEVs of pure CMB maps and bias corrected cleaned maps.

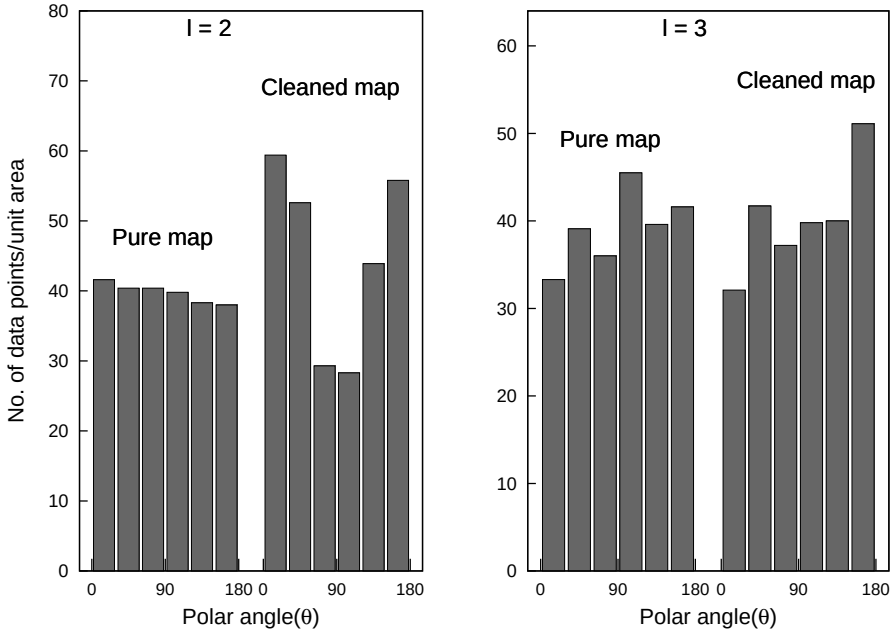

Figure 5: Distribution of the polar angle of PEVs for both the pure map and cleaned map, after bias correction, for $l = 2, 3$.

alignment in the cleaned maps. In Fig. [7] we show a plot of $(1-\cos(\alpha_{23,p}))$ vs $(1-\cos(\alpha_{23,c}))$ for all the 500 simulations. Here, the subscripts 'p' and 'c' stand for "pure" and "clean" simulated CMB maps, respectively. If there is any correlation it will show up in such a plot. But, this plot illustrates that there is no sign of preferred alignment.

We next compute the P-value or the probability that the alignment seen in data arises due to a random fluctuation directly from simulations. We determine the number of random realizations of CMB data which show better alignment in comparison to what is observed. The probability is obtained by dividing this number by the total number of random samples. Here we use both the randomly generated pure CMB maps as well as simulated foreground cleaned maps. For the bias corrected IPSE five year map we find that the probability is 0.004 if we use the simulated pure CMB maps. The probability remains unchanged if it is computed by using the simulated cleaned maps. The corresponding numbers for the seven year maps are 0.004 and 0.002 for the simulated pure CMB maps and the cleaned maps respectively. The result remains unchanged if we apply the residual foreground bias correction to the simulated cleaned maps. These results agree well with those given in Table 2.

Hence we find no evidence for any systematic effect which may cause alignment of PEVs, despite the presence of a systematic effect on power, C_l. We do find a systematic shift of the PEVs away from the galactic plane. However the final PEVs point in random directions. Hence rather than causing alignment, this effect has a tendency to distort any signal of alignment that might be present in the original sample.

As we have mentioned earlier, the negative bias does cause a systematic reduction of power for low l multipoles. This is seen clearly in Fig. [8] where we plot the sum of the eigenvalues of the power tensor for $l = 2, 3$ both for simulated pure and cleaned, bias corrected, maps. The sum of eigenvalues equals the total power, C_l, for each multipole. We find a systematic negative shift in the power for each random realization. After taking the average over all the simulations, we find that quadrupole power of the cleaned map is lower by 39 % in comparison to that of the pure CMB map. The corresponding octopole power gets reduced by 22 %.

We next assume that the alignment is caused by some effect other than foreground contamination. The foregrounds lead to a random shift in the PEVs causing a certain level of misalignment. Hence the angle between $l = 2$ and $l = 3$ PEVs must not be very small in comparison to the shift caused by foregrounds. The shift of the PEVs is quantified by the distribution plot shown in Fig. [3]. This should be associated with the randomness that the cleaning process introduces in the extraction of the PEV. We find that

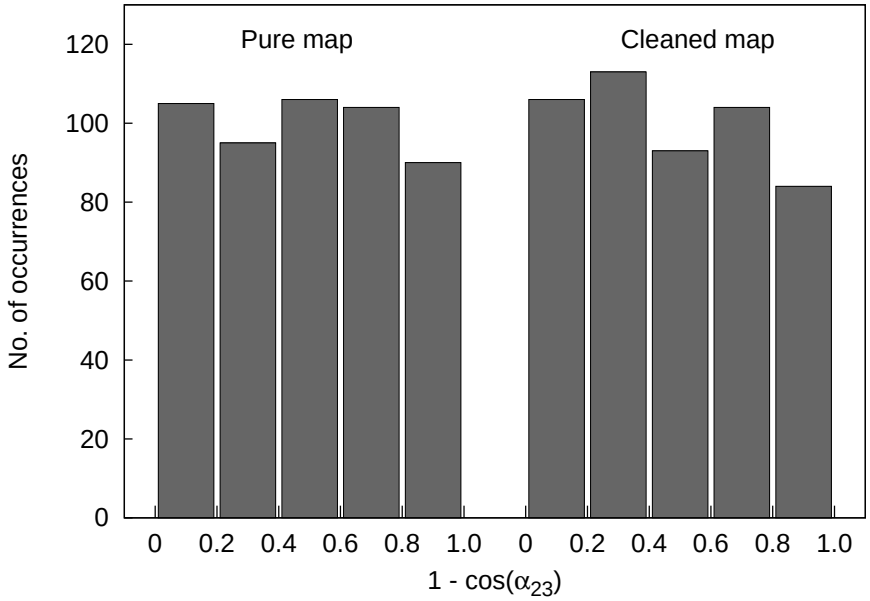

Figure 6: Distribution of $(1 - \cos(\alpha_{23}))$ where α_{23} is the angle between the quadrupole and octopole both for the pure map and the cleaned map, after bias correction.

probability of chance alignment for the IPSE cleaned five year and seven year map, after bias correction, is 0.0045 and 0.0027 respectively. We find that about 16% of the simulations have $(1 - \cos\alpha) < 0.0027$. At high galactic latitudes, corresponding to the Virgo alignment axis, this number is higher. It is reassuring that the number of random samples which show a shift in the PEV less than the observed alignment in the IPSE cleaned map is not too small.

5 Conclusions

We have studied the effect of foreground cleaning on the alignment of low l multipoles, $l = 2, 3$. It has been speculated in the past that the alignment may be caused by foreground contamination. The presence of residual foreground power in the cleaned CMB maps could lead to violation of statistical isotropy and hence alignment of low l multipoles. Furthermore, even in the case of perfect cleaning, the extracted power contains a negative bias, which is quite significant at low l. This has been shown explicitly in the case of the IPSE procedure. We anticipate the presence of such a bias also in the

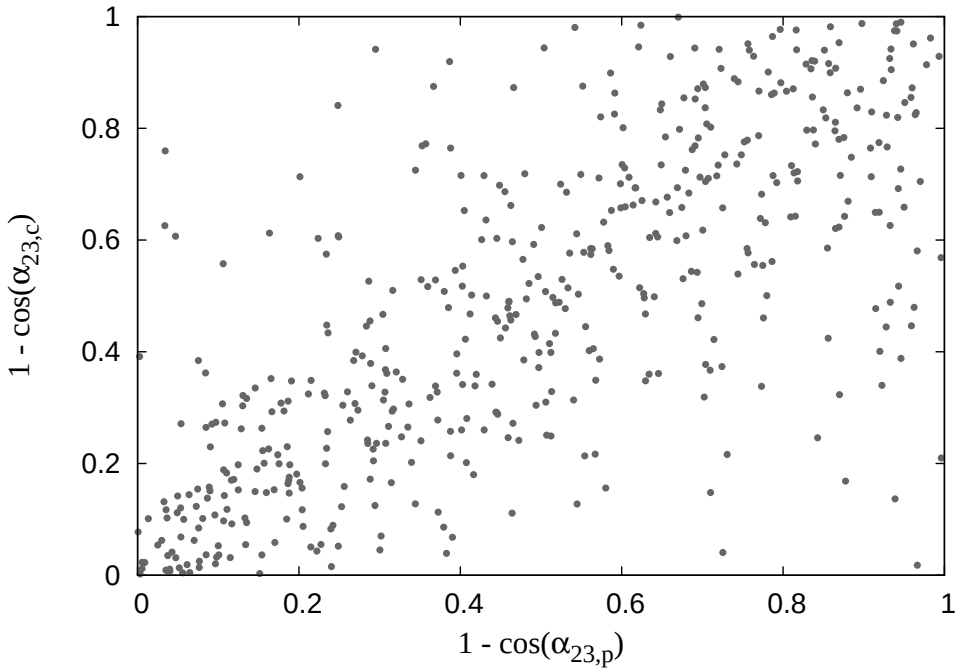

Figure 7: The alignment between quadrupole and octopole of pure map and bias corrected cleaned maps are plotted here, to find any correlations between them. On y-axis, is $1 - \cos(\alpha_{23,c})$, where $\cos\alpha_{23,c} = \hat{n}_{l2} \cdot \hat{n}_{l3}$ and $\hat{n}_{l2}$ and $\hat{n}_{l3}$ are the PEVs corresponding to $l = 2$ and $l = 3$, respectively, for the simulated foreground cleaned maps. On x-axis we have the same measure corresponding to the pure CMB maps.

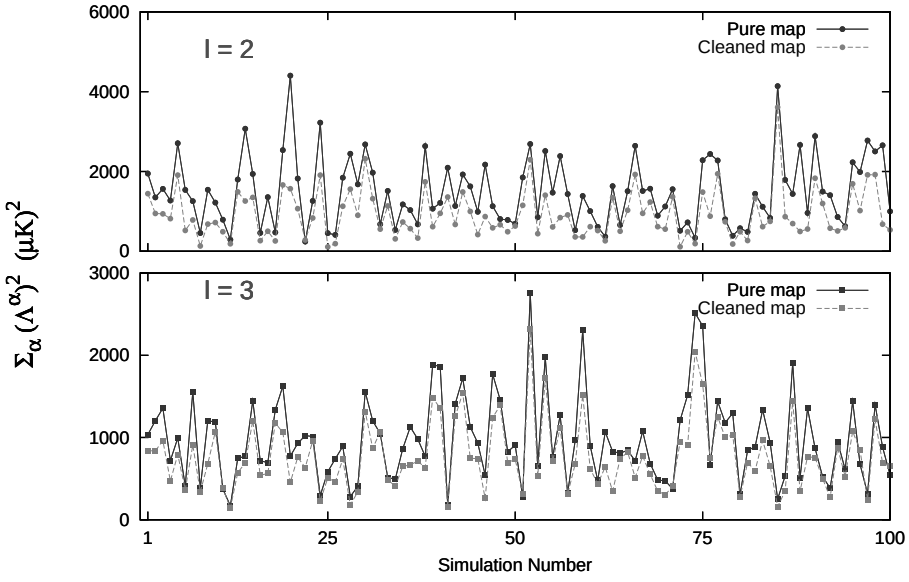

Figure 8: The sum of eigenvalues, or the total power, for $l = 2, 3$ for the simulated pure CMB and the cleaned CMB map, after bias correction. We see a systematic negative shift in the power for each of the simulated maps.

ILC map but this requires further study. Using the IPSE procedure, we analytically compute the power tensor using some simplifying assumptions. We find that its ensemble average is not proportional to an identity matrix due to the presence of the low l bias. Hence this implies a violation of statistical isotropy. We next perform detailed numerical simulations within the framework of the IPSE method to determine the effect of foregrounds on the observed alignment.

Our IPSE simulation results, obtained using 500 randomly generated samples, show that the PEVs extracted from foreground cleaned maps are generally in good agreement with those obtained from pure CMB maps. In most cases the shift in PEVs is observed to be small. The largest change is seen in the case of quadrupole. The shift is dominant for PEVs which initially lie close to the galactic plane. In general, we find that the PEVs tend to get pushed away from the galactic plane towards the galactic poles. Similar trend is also seen in the case of octopole but with much reduced significance. We do not, however, see any evidence for alignment among the quadrupole and octopole PEVs extracted from the foreground cleaned maps. The significance or P-values extracted by using simulated cleaned maps are found to be in good agreement with those obtained by using simulated pure CMB maps. These also show good agreement with the results obtained analytically and listed in Table 2.

Hence despite the systematic shift of PEVs away from the galactic plane, as observed dominantly in the case of quadrupole, we find that foregrounds do not cause alignment of quadrupole and octopole. This is because the change in PEVs due to foreground cleaning is generally small and mostly in random directions. One might be tempted to propose a scenario where the shift towards galactic poles is a much more significant effect which may be caused by the presence of much stronger level of foreground contamination. In this case it is conceivable that the PEVs extracted from the foreground cleaned maps would point dominantly towards the galactic poles and hence show alignment. However this would require a very large foreground contamination in comparison to currently accepted model. The level of contamination has to be sufficiently large so that both the quadrupole and octopole PEVs tend to align with the galactic poles. Although the quadrupole shows a somewhat significant shift of PEVs away from galactic plane, this trend is barely noticeable in the case of octopole. We emphasize that even in the case of quadrupole the shift of PEV is very small in most cases. Furthermore such a proposal will imply that the direction of alignment points towards the galactic poles which is not consistent with the observed axis. Hence we conclude that foreground contamination is very unlikely to cause the observed alignment.

Due to the random nature of the shift caused by foreground cleaning, it is more likely to cause misalignment of multipoles. We see this clearly by comparing the results using IPSE before and after removing the bias due to foreground contamination in the galactic plane. The alignment is found to be much stronger after removing the residual foreground bias which arises due to remnant foregrounds, present in our cleaned maps. It is extracted by simulations using the PSM for foregrounds and then removed from the cleaned map. Furthermore we see that alignment becomes much more significant as more data is accumulated. The alignment seen in seven year data, for example, is much better than seen in five year data which in turn is better than that seen in three year data. This is clearly caused by reduced uncertainties as more data accumulates. Hence we conclude that both the foregrounds and detector noise are more likely to distort, rather than cause, the signal of alignment.

Acknowledgements: P. K. Samal thanks NISER, Bhubaneswar for providing their computer and library facility.

References

Abramo L. R., Sodre Jr., L., Wuensche C. A., 2006, Phys. Rev., D 74, 083515

Ackerman L., Carroll S. M., Wise M. B., 2009, Phys. Rev., D 75, 069901

Armendariz-Picon C., 2004, JCAP, 7, 7

Battye R. A., Moss A., 2006, Phys. Rev., D 74, 041301

Bennett C. L. et al., 2003, ApJS, 148, 1

Berera A., Buniy R. V., Kephart T. W., 2004, JCAP, 10, 16

Bernui A., Villela T., Wuensche C. A., Leonardi R., Ferreira I., 2006, A&A, 454, 409

Bernui A., Mota B., Reboucas M. J., Tavakol R., 2007, A&A, 464, 479

Bielewicz P., Gorski K. M., Banday A. J., 2004, MNRAS, 355, 1283

Bielewicz P., Eriksen H. K., Banday A. J., Gorski K. M., Lilje P. B., 2005, ApJ, 635, 750

Birch P., 1982, Nature, 298, 451

Bouchet F. R., Gispert R., 1999, New Astronomy, 4, 443

Buniy R. V., Berera A., Kephart T. W., 2006, Phys. Rev., D 73, 063529

Carroll S. M., Tseng C.-Y., Wise M. B., 2010, Phys. Rev., D 81, 083501

Copi C. J., Huterer D., Schwarz D. J., Starkman G. D., 2006, MNRAS, 367, 79

Copi C. J., Huterer D., Schwarz D. J., Starkman G. D., 2007, Phys. Rev., D 75, 023507

Cruz M., Martinez-Gonzalez E., Vielva P., Cayon L., 2005, MNRAS, 356, 29

de Oliveira-Costa A., Tegmark M., Zaldarriaga M., Hamilton A., 2004, Phys. Rev., D 69, 063516

de Oliveira-Costa A., Tegmark M., 2006, Phys. Rev., D 74, 023005

Delabrouille J., Cardoso J. F., 2009, Data Analysis in Cosmology, Lecture notes in physics 665, eds Vicent J. Martinez et al. (Springer), pages 159-205

Erickcek A. L., Hirata C. M., Kamionkowski M., 2009, Phys. Rev., D 80, 083507

Eriksen H. K., Hansen F. K., Banday A. J., Gorski K. M., Lilje P. B., 2004, ApJ, 605, 14

Eriksen H. K., Banday A. J., Gorski K. M., Hansen F. K., Lilje P. B., 2007, ApJ, 660, L81

Freeman P. E., Genovese C. R., Miller C. J., Nichol R. C., Wasserman L., 2006, ApJ, 638, 1

Gold B. et.al., 2010, arXiv:1001.4555

Gordon C., Hu W., Huterer D., Crawford T., 2005, Phys. Rev., D 72, 103002

Hajian A., Souradeep T., Cornish N., 2005, ApJ, 618, L63

Hajian A., Souradeep T., 2006, Phys. Rev., D 74, 123521

Hansen F. K., Banday A. J., Gorski K. M., 2004, MNRAS, 354, 641

Helling R. C., Schupp P., Tesileanu T., 2006, Phys. Rev., D 74, 063004

Hill R. S. *et al*, 2008, arXiv:0803.0570

Hinshaw G. et al., 2007, ApJS, 170, 288

Hoftuft J., Eriksen H. K., Banday A. J., Gorski K. M., Hansen F. K., Lilje P. B., 2009, ApJ, 699, 985

Hutsemékers D., 1998, A&A, 332, 410

Hutsemékers D., Lamy H., 2001, A&A, 367, 381

Inoue K. T., Silk J., 2006, ApJ, 648, 23

Itoh Y., Yahata K., Takada M., 2009, arXiv:0912.1460

Jain P., Ralston J. P., 1999, Mod. Phy. Lett. A, 14, 417

Jain P., Narain G., Sarala S., 2004, MNRAS, 347, 394

Kahniashvili T., Lavrelashvili G., Ratra B., 2008, Phys. Rev., D 78, 063012

Kashlinsky A., Atrio-Barandela F., Kocevski D., Ebeling H., 2008, ApJ, 686, L49

Kashlinsky A., Atrio-Barandela F., Kocevski D., Ebeling H., 2009, ApJ, 691, 1479

Katz G., Weeks J., 2004, Phys. Rev., D 70, 063527

Koivisto T., Mota D. F., 2008, ApJ, 679, 1

Land K., Magueijo J., 2006, MNRAS, 367, 1714

Land K., Magueijo J., 2007, MNRAS, 378, 153

Magueijo J., Sorkin R. D., 2007, MNRAS, 377, L39

Moffat J. W., 2005, JCAP, 10, 12

Naselsky P. D., Verkhodanov O. V., Nielsen M. T. B., 2008, Astrophys. Bull., 63, 216

Prunet S., Uzan J., Bernardeau F., Brunier T., 2005, Phys. Rev., D 71, 083508

Rakić A., Rasanen S., Schwarz D. J., 2006, MNRAS, 369, L27

Rakić A., Schwarz D. J., 2007, Phys. Rev., D 75, 103002

Ralston J. P., Jain P., 2004, Int. J. of Mod. Phys., D 13, 1857

Rodrigues D. C., 2008, Phys. Rev., D 77, 023534

Saha R., Prunet S., Jain P., Souradeep T., 2008, Phys. Rev., D 78, 023003

Saha R., Jain P., Souradeep T., 2006, ApJL 645, L89

Samal P., Saha R., Delabrouille J., Prunet S., Souradeep T., 2010, ApJ, 714, 840

Samal P. K., Saha R., Jain P., Ralston J. P., 2008, MNRAS, 385, 1718

Samal P. K., Saha R., Jain P., Ralston J. P., 2009, MNRAS, 396, 511

Sarkar D., Huterer D., Copi C. J., Starkman G. D., Schwarz D. J., 2010, arXiv:1004.3784

Schwarz D. J., Starkman G. D., Huterer D., Copi C. J., 2004, PRL, 93, 221301

Slosar A., Seljak U., 2004, Phys. Rev., D 70, 083002

Tegmark M., Efstathiou, G., 1996, MNRAS 281, 1297

Tegmark M., de Oliveira-Costa A, Hamilton A. J., 2003, Phys. Rev., D 68, 123523

Wiaux Y., Vielva P., Martinez-Gonzalez E., Vandergheynst P., 2006, PRL, 96, 151303